

Spin-dependent transmission of low-energy electrons through ultrathin magnetic layers

Y. Lassailly, H.-J. Drouhin, A. J. van der Sluijs, and G. Lampel

*Laboratoire de Physique de la Matière Condensée, Centre National de la Recherche Scientifique,
Ecole Polytechnique, 91128 Palaiseau, France*

C. Marlière

Institut d'Optique Théorique et Appliquée, Centre National de la Recherche Scientifique, 91403 Orsay, France

(Received 19 August 1994)

We present an experiment in which the attenuation of a spin-polarized free electron beam is measured by direct transmission through an ultrathin ferromagnetic layer. The self-supported metal target consists of a 1-nm-thick cobalt film sandwiched between 21- and 2-nm-thick gold layers. Measurements are performed throughout a wide energy range (incident electron energies from 4 eV to 50 eV above the Fermi level). At low energy, close to the clean surface vacuum level, we find that the transmission coefficient of minority spin electrons is about 0.7 times that of majority spin electrons.

Magnetic layers in the nanometer range, sandwiched between nonmagnetic metal films, appear today as very promising systems for high-density recording and are studied in many laboratories. A great deal of attention has been paid to giant magnetoresistance in multilayers.¹ Modeling is based on transport properties of electrons with different spin orientations at the Fermi surface. Both semiclassical and full-quantum models consider bulk and interface scattering, thus introducing several fitting parameters. They lead to the conclusion that the transmission coefficients of electrons with spin parallel or antiparallel to the layer magnetization are strongly different.

Spin-polarized electron photoemission spectroscopy also probes magnetism, at the monolayer scale. Spin-dependent transmission of low-energy electrons through ferromagnetic layers is often investigated by electron emission from a nonmagnetic substrate into a ferromagnetic overlayer, which allows the determination of spin-dependent inelastic mean free paths (IMFP's).² Even though the main features of these effects are qualitatively established, the nature of the significant interactions remains an open question. The photoemission approach is connected to the old but still controversial problem of the quantitative understanding of electron transport in metals: at very low energy, the IMFP is known to be very large (from the conductivity relaxation time) but it reaches minimum values (a few tenths of nm) for energies of the order of 100 eV.³ A pioneering experimental investigation was performed by Kanter,⁴ who studied the transmission of electrons (about 5–10 eV above the Fermi energy) through 15–40-nm-thick polycrystalline gold, aluminum, and silver foils supported by electron microscope specimen screens. His results seem to be sustained by some photoemission measurements⁵ and by lifetime widths deduced from inverse photoemission.⁶ Nevertheless, data at very low energy, on well-controlled systems, remain dramatically scarce; it appears that the IMFP cannot be obtained from a “universal curve,” as was thought in the past, but is material dependent;⁷ its large increase when lowering the electron energy near the clean surface vacuum level, directly observed only in Ref. 4, remains questionable.²

Today, progress in thin-film technology and industrial challenges related to thin-film magnetism give a new impulse to transmission experiments. In the present paper we report on a truly direct investigation of spin-dependent interactions in low-energy electron transport in metals, based on energy-resolved transmission of spin-polarized electrons through ultrathin, self-supported magnetic structures. The main result is that the transmission of spin-polarized electrons is *highly* dependent on the state of magnetization of the target.

Here, the sample is an ultrathin cobalt layer embedded between thicker gold layers. This system is well known as a model system for perpendicular magnetization. Thin films are grown at room temperature by thermal (Au) or electron-beam (Co) evaporation under ultrahigh vacuum. An intermediate layer of amorphous NaCl is first deposited on a float glass substrate, then an Au film (21 nm thickness) is evaporated and annealed up to 150 °C. *In situ* x-ray reflectometry, reflection high-energy electron diffraction, *ex situ* x-ray diffraction, and transmission electron microscopy show that the resulting gold film has a geometrical and crystallographic structure very similar to that obtained when directly deposited on float glass: the rms value of the surface roughness is about 0.4 nm; the film is polycrystalline but textured with the (111) close-packed planes parallel to the substrate surface.⁸ Then Co (1 nm) and a second Au layer (2 nm) are evaporated at room temperature. The square hysteresis loops measured by Faraday rotation are identical to those measured on Au/Co/Au sandwiches with similar thickness directly deposited on float glass.⁹ Subsequently the layered structure is lifted off in water, deposited onto a molybdenum aperture (a few mm diameter), and the sample is introduced into the experiment chamber (base pressure in the 10⁻¹¹ Torr range) with moderate bakeout (<150 °C). It was confirmed by magneto-optical measurements that this procedure does not alter the magnetic properties of the sample; furthermore, inspection by atomic force microscopy of a check sample redeposited on a glass plate after lift-off showed no indication of pin holes.

The experimental setup is described in Fig. 1. Its principal elements are a spin-polarized electron source, transport op-

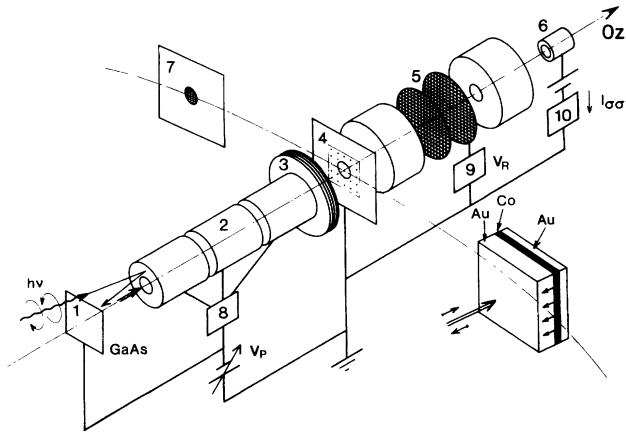


FIG. 1. Experimental setup: 1, photocathode; 2, transport optics; 3, coaxial coil; 4, sample; 5, retarding grids; 6, Faraday cup; 7, gold grid; 8, electron optics power supply; 9, retarding potential (V_R) control; 10, current detection; the bias potential V_P defines E_P . In the zoom on the sample, spin configurations are indicated by the arrows.

tics, and a retarding-field energy analyzer. The longitudinally spin-polarized electron beam impinges normally on the sample's thicker gold layer. The electron source is a negative electron affinity GaAs photocathode, which provides a high intensity with a low energy dispersion.¹⁰ It is optically pumped by a laser diode (wavelength 800 nm); the light is circularly polarized using a Pockels electro-optical modulator operated at about 800 Hz. The light helicity was determined using a reference quartz quarterwave plate. From luminescence measurements, we deduce an emitted electron polarization $P \approx 0.24$.¹⁰ The transport optics is a three cylinder electrostatic lens, ended by a diaphragm, which defines a uniform electric field at the sample. A coaxial coil, located at the end of the optics, allows layer magnetization perpendicular to the surface and magnetization reversal in the measurement configuration. Current is pulsed through the coil to produce the saturation field. The current transmitted through the sample is energy analyzed using a retarding-field analyzer (resolution ~ 200 meV). The sample is grounded and the analyzer potentials are fixed (except for the retarding grids) with respect to the ground potential. The photocathode and transport optics potentials are shifted with respect to the sample potential, thus defining the primary electron energy E_P . The transmitted current is either directly detected or its polarization dependence is measured through a lock-in amplifier. In the latter case, care was taken to reduce stray modulations below a few times 10^{-4} : these parasitic effects involve both the circularly modulated optical excitation and the electron transport towards the sample. The best way to reduce them was to control the current absorbed by the sample: because the current is essentially absorbed in the 21-nm gold layer, no spin dependence is expected.

Figure 2 shows the transmitted current as a function of the retarding potential, for E_P ranging from 4.3 eV to 9.6 eV above the Fermi level. At higher E_P , the main features of the curves do not change. Two types of structures can be observed. The high-energy edge, whose position varies linearly

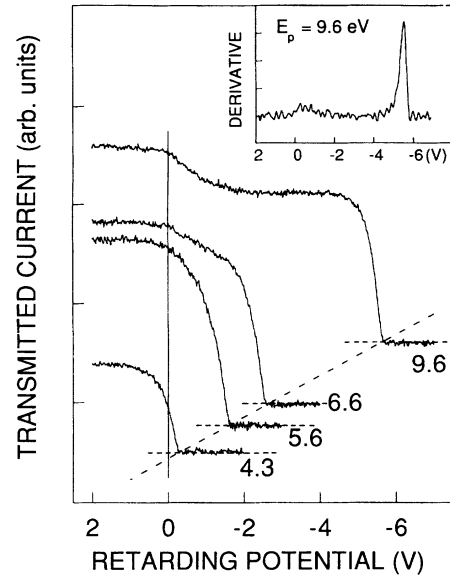


FIG. 2. Transmitted current versus retarding potential for primary energies E_P from 4.3 eV up to 9.6 eV, referred to the target Fermi level; the Au work function has been taken equal to 4 eV, a value deduced from these measurements and from the mean energy of the electrons emitted from a GaAs photocathode (Ref. 10). The curves are normalized to the incident current. Their zero signal levels (dotted lines) are shifted by an amount proportional to E_P . The dashed straight line visualizes the high-energy edge, originating from ballistic electrons; the vertical line corresponds to the low-energy end, i.e., to the target vacuum level. The inset shows the derivative of the 9.6-eV curve, that is the corresponding electron energy distribution.

with E_P , corresponds to ballistic electrons, or to electrons which essentially experienced elastic scattering throughout the foil ("quasielastic" part). The low-energy step ("inelastic" part) originates from electrons which have lost a notable part of their energy or from true secondary electrons, emitted with a negligible kinetic energy, at the surface vacuum level (with possible accumulation in some conduction band minima). The relative intensities of these two contributions depend on E_P ; when $E_P < 6$ eV, the inelastic part cannot be separately distinguished. The total transmitted current is of the order of 10^{-5} of the primary beam; this is consistent with an IMFP of the order of 2 nm (in rough agreement with Ref. 7) and nearly energy independent.² However, the acceptance of the collecting optics varies with E_P . As a consequence, in this paper we do not quantitatively analyze the total transmission of low-energy electrons through the sample but rather concentrate on the differential spin transmission.

Figure 3 shows a transmission curve as a function of the retarding potential for $E_P = 9.6$ eV and also the spin-dependent differential transmitted current (DTC) $\Delta I_{\sigma\sigma'} = (I_{\sigma\sigma'} - I_{-\sigma\sigma'})$, where $I_{\sigma\sigma'}$ is the transmitted current for incident electron spin polarization parallel ($\sigma = +$) or antiparallel ($\sigma = -$) to the beam propagation axis Oz and for majority spin in the ferromagnet parallel ($\sigma' = +$) or antiparallel ($\sigma' = -$) to Oz . The measurements were repeated for the two opposite magnetizations of the layer. The symmetry of the two resulting curves with respect to the zero signal level excludes any instrumental asymmetry. Figure 4 presents a set

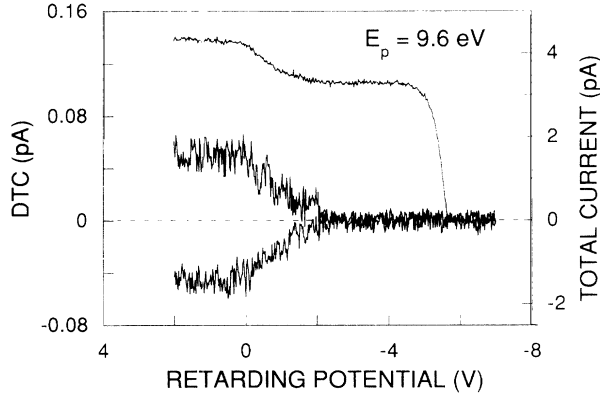


FIG. 3. Transmitted current (upper curve) and the corresponding DTC's for an incident current equal to $0.36 \mu\text{A}$ and $E_p = 9.6 \text{ eV}$. The DTC's have been measured for two opposite magnetizations of the cobalt layer [lower curves; the positive (negative) signal corresponds to $\sigma' = +$ ($\sigma' = -$)].

of DTC's. Striking features are the large difference in transmission between the two incident spin orientations at low E_p and its sharp decrease at high E_p . At low primary energy, the incident electrons are transmitted at an energy close to the $3d$ bands, and spin-dependent transmission is observed whatever the emerging electron energy. On the contrary, for $E_p > 8 \text{ eV}$, spin-dependent transmission only appears at the inelastic step. Intermediate cases are possible, with a small DTC in the elastic part. We define the experimental transmission asymmetry for a given E_p as

$$\mathcal{A}^\alpha(E_p) = \frac{I_{\sigma\sigma}^\alpha(E_p) - I_{-\sigma\sigma}^\alpha(E_p)}{I_{\sigma\sigma}^\alpha(E_p) + I_{-\sigma\sigma}^\alpha(E_p)}.$$

The index α refers to the analyzing conditions: in the following, $\mathcal{A}^{\text{el}}(E_p)$ is measured when the retarding voltage se-

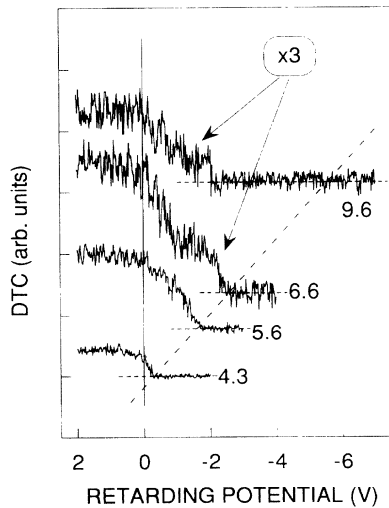


FIG. 4. DTC's versus retarding potential for different incident electron energies. The curves are normalized to the incident current; for clarity, the two upper curves have been magnified by a factor of 3. The representation is similar to the one used in Fig. 2

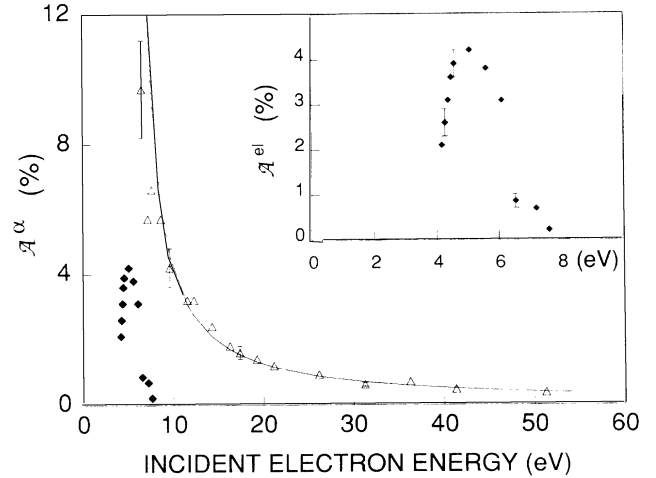


FIG. 5. Transmission asymmetries $\mathcal{A}^{\text{el}}(E_p)$ (\blacklozenge) and $\mathcal{A}^{\text{in}}(E_p)$ (\triangle) versus primary electron energy E_p . The solid line is the phenomenological fit $\mathcal{A}^{\text{in}}(E_p) \approx 18(E_p - 5.8)^{-1}$. The inset is a zoom on the $\mathcal{A}^{\text{el}}(E_p)$ curve.

lects only the quasielastic step and similarly $\mathcal{A}^{\text{in}}(E_p)$ corresponds to the inelastic part. Their variations versus E_p are plotted in Fig. 5.

In the *quasielastic* DTC part, the initial conditions at the Co layer are well defined; the mean free path for spin relaxation is much longer than that for energy relaxation, so that the spin polarization is conserved after passing the Au layer.^{7,11} We define the transmission factors through the Co layer at energy E as $T_\pm(E)$ for impinging electrons with spins parallel (antiparallel) to the majority spins in the magnetic layer of thickness d . Neglecting interface effects, $T_\pm(E) = \exp[-d/\lambda^\pm(E)]$ where $\lambda^+(E)$ [$\lambda^-(E)$] is the IMFP for majority (minority) spin electrons. It is then straightforward to show that

$$\begin{aligned} \mathcal{A}^{\text{el}}(E_p) &= P \frac{[T_+(E_p) - T_-(E_p)]}{[T_+(E_p) + T_-(E_p)]} \\ &= P \tanh \left[\frac{d}{2} \left(\frac{1}{\lambda^-} - \frac{1}{\lambda^+} \right) \right]. \end{aligned}$$

From the peak asymmetry around 5 eV, we deduce that $T_-/T_+ = [P - \mathcal{A}^{\text{el}}(E_p)]/[P + \mathcal{A}^{\text{el}}(E_p)] \approx 0.7$; electrons with spin parallel to the majority spin direction are then more easily transmitted. This can be qualitatively understood since there is a larger number of empty states near the Fermi level for minority spin electrons, thus more allowed relaxation channels. Note that here the relevant physical quantity is the ratio T_-/T_+ , which characterizes the spin asymmetry, and not the IMFP's, which are not independently measured. However, to make comparisons to other published matter, a discussion in terms of IMFP's is useful. In line with results obtained at the Fermi level,¹² we might assume $\lambda^- \ll \lambda^+$. The relation $[(1/\lambda^-) - (1/\lambda^+)]d/2 \approx \mathcal{A}^{\text{el}}(E_p)/P$ would then yield $\lambda^- \approx 2.9 \text{ nm}$. This would imply a much too large value for λ^+ , thus a too small attenuation for an unpolarized electron beam (the IMFP in Co should be much smaller than in Au).⁷ The assumption $\lambda^- \ll \lambda^+$ must therefore be rejected.

On the other hand, our result is consistent with IMFP's of the order of 1 nm, with a spin asymmetry $(\lambda^+ - \lambda^-)/(\lambda^+ + \lambda^-)$ close to 20%. Qualitatively, this agrees with published results.^{2,7,13,14} Nevertheless, the observed rapid decrease of the spin asymmetry with energy, expected from Ref. 14, was not found in Refs. 2 and 13. This could be due to the interface contribution but requires further investigation. The origin of the asymmetry reduction at the low-energy side is not understood yet.

Surprisingly, $\mathcal{A}^{\text{in}}(E_P)$ is much larger than $\mathcal{A}^{\text{el}}(E_P)$. One could expect that the higher-energy primary electrons first relax only their energy, at a different rate for majority and minority spin electrons, and then undergo spin-dependent transport towards the interface, but the magnitude of the effect can hardly be explained this way. When increasing E_P , the contribution of secondary electrons becomes significant and these electrons, which are spin polarized as they reflect the bulk magnetization,¹⁴ have lost the memory of the primary beam polarization so that the transmission asymmetry is reduced. However, electrons travel throughout a complicated layered structure, with possible spin-dependent surface and interface reflections, so that measurements in other configurations and preparation conditions are necessary before drawing definite conclusions; spin analysis of the transmitted current would constitute a crucial test of the models developed to describe the inelastic region.¹⁴

We observe that the literature refers to two different classes of experiments: the first one involves phenomena arising at a few eV above the vacuum level of the clean surface (photoemission experiments), while the second one

involves phenomena arising at the Fermi level (magnetotransport). The first kind of experiments yields a small asymmetry in the IMFP's, whereas the other type of experiments may provide an order of magnitude difference between λ^+ and λ^- .¹² It should also be noted that the mean free path deduced from transport experiments is associated with momentum relaxation, i.e., elastic collisions. The experiments reported here are of the first type; lowering the work function of both sides of the metal target by cesium deposition will allow probing of lower energies, bridging a gap in the experimental data. Although we do not observe any significant increase of the IMFP for electrons with energies slightly exceeding the vacuum level of the clean surface, the high efficiency (a few tenths of a percent) obtained from field-assisted Ag/InP photoemitters,¹⁵ through a 10-nm-thick silver layer, demonstrates that the IMFP for electrons at 1–2 eV above the Fermi level is of the order of 5 nm. This energy domain is within the scope of transmission experiments, which allow the investigation of a wide energy range, offering more capabilities than all-solid-state structures for both injection and analysis.¹² Finally, we would like to point out the possible implications of this work for the development of solid-state spin detectors.⁷

We are grateful to J.-P. Renard and his group for many fruitful discussions and for a continuous interest. We thank J.-P. Chauvineau for his support. We are indebted to D. M. Campbell, C. Hermann, and J.-P. Renard for a critical reading of the manuscript. H.-J.D. thanks the "Direction des Recherches, Etudes et Techniques de la Délégation Générale pour l'Armement" for support.

¹E. Vélú *et al.*, Phys. Rev. B **37**, 668 (1988); M. N. Baibich *et al.*, Phys. Rev. Lett. **61**, 2472 (1988).

²D. P. Pappas *et al.*, Phys. Rev. Lett. **66**, 504 (1991).

³M. P. Seah and W. A. Dench, Surf. Interface Anal. **1**, 2 (1979).

⁴H. Kanter, Phys. Rev. B **1**, 522 (1970).

⁵D. Norman and D. P. Woodruff, Solid State Commun. **22**, 711 (1977), and references therein.

⁶A. Goldmann, W. Altmann, and V. Dose, Solid State Commun. **79**, 511 (1991).

⁷G. Schönhense and H. C. Siegmann, Ann. Phys. (Leipzig) **2**, 465 (1993).

⁸C. Marlière, D. Renard, and J.-P. Chauvineau, Thin Solid Films **201**, 317 (1991), and references therein.

⁹J. Ferre *et al.*, Appl. Phys. Lett. **56**, 1588 (1990).

¹⁰H.-J. Drouhin, C. Hermann, and G. Lampel, Phys. Rev. B **31**, 3859 (1985); **31**, 3872 (1985).

¹¹F. Meier, G. L. Bona, and S. Hüfner, Phys. Rev. Lett. **52**, 1152 (1984).

¹²B. A. Gurney *et al.*, Phys. Rev. Lett. **71**, 4023 (1993).

¹³M. Getzlaff, J. Bansmann, and G. Schönhense, Solid State Commun. **87**, 467 (1993).

¹⁴D. R. Penn, S. P. Apell, and S. M. Girvin, Phys. Rev. B **32**, 7753 (1985).

¹⁵J. Peretti, H.-J. Drouhin, and D. Paget, Phys. Rev. Lett. **64**, 1682 (1990).